MSUCL-240
May 1977

The (p,t) and (p,^{3}He) Reactions on ^{39}K*

H. Nann and B. H. Wildenthal

Cyclotron Laboratory and Department of Physics
Michigan State University, East Lansing, Mich. 48824

Angular distributions of the ^{39}K(p,t)^{37}K and ^{39}K(p,^{3}He)^{37}Ar reactions between 3° and 55° have been measured at 40 MeV bombarding energy. The experimental differential cross sections of the transitions to several of the low-lying mirror pairs of even-parity final states in ^{37}K and ^{37}Ar are compared to results of microscopic distorted-wave Born approximation (DWBA) calculations based on current shell-model wave functions. The sensitivity of these DWBA calculations to optical model parameters is studied. It is found out that a satisfactory test of the shell-model wave functions used in the analysis can be obtained provided that the DWBA calculations describe the shapes of the observed angular distributions well.

NUCLEAR REACTIONS ^{39}K(p,t), ^{39}K(p,^{3}He), E_p=40 MeV; measured $\sigma(E_t, E_{^3He}, \theta)$; natural target; DWBA analysis.

*Work supported in part by the U.S. National Science Foundation

I. Introduction

The different selectivity of the (p,t) and (p,^{3}He) reactions on T_z=1/2 target nuclei leading to mirror final states can be used, in principle, to test different parts of the initial and final states wave functions. In practice, however, uncertainties in the distorted-wave Born approximation (DWBA) calculations tend to mask the distinctive features and leave the analysis to some degree ambiguous.

The present ^{39}K(p,t) and ^{39}K(p,^{3}He) work is part of a systematic investigation of the (p,t) and (p,^{3}He) reactions on T_z=1/2 nuclei in the 2s-1d shell[1,2] with the aim of testing the two-particle correlations in current shell-model wave functions. For the initial and final nuclei several sets of shell-model wave functions exist[3,4] which were calculated in the full $1d_{5/2}$-$2s_{1/2}$-$1d_{3/2}$ vector space. One set of calculations[3] uses two-body matrix elements derived by reaction matrix techniques from the Hamada-Johnstone nucleon-nucleon scattering potential. In recent calculations[4] the two-body matrix elements were treated as independent free parameters adjusted to fit experimental ground state binding energies and level spacings.

Based on these shell-model wave functions, DWBA calculations have been carried out and compared to the experimental data. The structure of most of the nuclear states involved is rather simple. Thus, the effects of the uncertainties in the DWBA calculations, such as optical model parameters or form factor descriptions, upon the conclusions which can be drawn about the wave functions used in the analysis can be studied.

II. Experimental Procedure and Results

The experiments were carried out with a 40 MeV proton beam from the Michigan State University cyclotron. The reaction products were momentum analysed in an Enge split-pole magnetic spectrograph and detected in the focal plane with a position sensitive resistive-wire-proportional counter plastic-scintillator combination. This equipment provided excellent particle identification and an energy resolution of about 30 keV. The targets were made by evaporating natural potassium metal (93% ^{39}K and 7% ^{41}K) onto thin carbon backings. These targets were kept under vacuum throughout the experiment. The target thicknesses ranged from 35 to 150 $\mu g/cm^2$. A NaI scintillation counter placed in the scattering chambers at 90° allowed continuous monitoring of the target conditions and the normalization of the relative cross sections at different angles.

The relative (p,t) to (p,^{3}He) cross sections were measured during the same experimental run, with the same configuration of target, beam, and detector system. Only the magnetic field of the spectrograph was changed in order to bring the triton and ^{3}He particles to the same position on the focal plane. The error in the relative (p,t) to (p,^{3}He) cross section is estimated to be less than 10%. The absolute cross section normalization for the (p,t) and (p,^{3}He) data was taken relative to the elastic proton scattering cross section in the angular region from 25° to 50°. Again an identical experimental configuration was used for these different measurements. The measured elastic cross sections were assumed to have the values calculated in the optical model from the parameters of Becchetti and Greenlees[5]. The accuracy of the absolute differential cross section is estimated to be about 20%.

Figure 1 shows spectra from the $^{39}K(p,t)^{37}K$ reaction in the upper half and from the $^{39}K(p,^3He)^{37}Ar$ reaction in the lower half. Only the even parity states in the final nuclei are populated with reasonable strength. Group due to contaminants are hatched.

The measured differential cross sections are shown in Figs. 6 and 7. The error bars reflect only statistical uncertainties. In the upper halves the $^{39}K(p,t)^{37}K$ results are displayed, while the $^{39}K(p,^3He)^{37}Ar$ results to the corresponding mirror levels are exhibited in the lower halves. The curves shown are results from DWBA calculations and will later be discussed in detail.

III. Distorted-Wave Analysis

A. General Remarks

The microscopic distorted-wave Born approximation (DWBA) calculations have been performed with the code DWUCK. The cross section for the two-nucleon pick-up reaction is given by (see Refs. 6,7)

$$\frac{d\sigma}{d\Omega} = D_o^2 \cdot \epsilon \sum_{LSJT} b_{ST}^2 \, (T_B N_B T N \, T_A N_A)^2 \, |D(S,T)|^2 \, \sigma_{LSJT}^{DWBA}(\theta)$$

Here L,S,J,T are the quantum numbers of the transferred nucleon pair. The factor b_{ST}^2 is a spectroscopic factor for the light particles. The function D(S,T) depends upon the strength of the spin-isospin exchange terms in the interaction potential. The quantity D_o^2 is the normalization factor which arises in making the zero-range approximation. The factor ϵ deals with the goodness of the wave function description of the initial and final states and will be used to compare experimental transition

strengths to those calculated from the nuclear wave functions used in the analysis. Disagreement between theory and experiment is indicated by deviations of this factor ϵ from unity.

B. Optical-Model Parameter Sensitivity

In previous analyses of two-nucleon transfer reactions a strong sensitivity of DWBA calculations to the choice of the optical-model parameters has been noted[1]. Therefore we performed a series of calculations using different optical-model parameters available from the literature.

As a first choice we took the proton optical-model parameters from the average set of Becchetti and Greenlees (BG)[5]. These parameters fit quite well the elastic scattering data as it is displayed in Fig. 2. For the triton and ^{3}He potentials an average set from the analysis of Urone et al.[8] (UPCR) was taken. Using these parameter sets DWBA calculations to the ground and excited states in the $^{39}K(p,t)^{37}K$ and $^{39}K(p,^3He)^{37}Ar$ reactions were carried out. The results are compared in Fig. 3 (full curve) to the experimental data. The fits are not very good, especially at the very forward angles. In addition, for the ground state transitions the position of the calculated first minimum is shifted by several degrees to larger angles compared to the experimental data.

Since the optical-model parameters for protons are quite well determined over a wide range of nuclei and energies, we kept them fixed and tried all available mass-3 optical parameters in an attempt to improve the fits to the experimental data. Somewhat surprisingly we found only small changes in the shapes of the angular distributions and were not able to improve the fits to the experimental data.

As a next step, several other proton optical-model parameters from the literature were used in the DWBA calculations. It turned out that the proton parameters from an analysis of Watson et al.[9] (WSS) combined with the UPCR mass-3 parameter set[8] improved the fits to the experimental data considerably (dashed curves in Fig. 3). It should be noted, however, that the WSS parameters do not describe the elastic scattering cross section as well as the BG parameter do (see dashed curve in Fig. 2).

Finally we used the proton and mass-3 optical parameters which gave good fits in previous analyses.[1,2] These parameters were adapted from the works of Greenlees and Pyle (GP)[10] and Morsch and Santo (MS)[11]. The fits to the experimental data are quite good (see dashed-dotted curves in Fig. 3). However, the GP proton parameter give a rather poor description of the elastic scattering data as can be seen in Fig. 2 (dashed-dotted curve).

Inspection of Fig. 3 shows that either the WSS-UPCR or the GP-MS parameter combination fits the experimental data equivalently well, although the two different combinations lead to different magnitudes of the differential cross sections. However, the relative cross sections for different transitions agree to within 10%. The parameter sets discussed above are listed in Table I.

In search for a better understanding of the observed optical model parameter sensitivity, the partial wave decomposition of the scattering amplitudes and the DWBA radial integrals were studied in some detail. As the test case, the L=0 transfer part of the $^{39}K(p,t)^{37}K$ ground state transition was choosen. Figure 4 shows the reflection coefficients calculated with the different optical-model parameter sets. The three

proton parameter sets BG, WSS and GP give quite different reflection coefficients, whereas the differences between the mass-3 parameter sets UPCR and MS are quite small. From this figure it is obvious that the difference $|L_p - L_t| \approx 5$ is much larger than the transferred orbital angular momentum L=0 implying appreciable momentum mismatching. This means that sizeable contributions to the transfer cross section come from the low partial waves. Figure 5 shows the partial wave decomposition of the DWBA radial integral for the three parameter-set combinations discussed above for the entrance and exit channels. Although the momentum matching is rather poor, the angular momentum localization is fairly sharp. One striking feature observed is that for the WSS-UPCR and GP-MS parameter set cominations the contribution from the L=5 partial wave is reduced. Most probably it is this suppression which improves the fits of the angular distributions at very forward angles. It should be noted that the introduction of a radial cutoff of 3.2 fm used in the calculations with the BG-UPCR potential set combination results also in a reduction of the contribution from the L=5 partial wave and consequently in a better fit to the experimental data at the very forward angles.

In summary, the present DWBA calculations with the well established proton parameters of Becchetti and Greenlees[5] tend to predict larger contributions from lower partial waves than the experimental data imply. At the moment it is not certain that this difficulty cannot be removed by a different choice of mass-3 optical parameters so that the contributions from the lower partial waves (especially in this case from the L=5 partial wave) are quenched by phase averaging. However, as it is shown later, it does not seem necessary for the extraction of reliable structure

information from the experimental data that the optical-model parameters used in the DWBA calculations fit the elastic scattering data exactly. It appears adequate merely that the DWBA results give reasonable fits to the experimental data.

C. Form Factor Description

The two-nucleon form factor was obtained by two different methods starting from single particle wave functions calculated in a Woods-Saxon well. In the first method, described by Drisko and Rybicki[12], these wave functions are expanded in terms of harmonic oscillator wave functions and the center-of-mass (c.m.) motion is projected out using the Talmi-Moshinky transformation. In the second method, described by Bayman and Kallio[13], the transformation to relative and c.m. coordinates is performed directly on the Woods-Saxon wave functions in the limit of zero relative angular momentum.

In order to compare these two form factor descriptions, DWBA calculations with the optical parameter set combination GP-MS were carried out using the spectroscopic amplitudes (see Table II) from the 12.5 p + ^{17}O wave function of Ref. 3. The form factors calculated by the two methods lead to nearly identical differential cross sections with respect to both the shape and the magntiude. For calculating the absolute values of the cross sections with the Bayman and Kallio form factor description the normalization procedure of Baer et al.[7] was imployed.

Since the Bayman and Kallio method of deriving the two-nucleon transfer form factor is already incorporated into the DWBA code DWUCK and therefore easier to use, all further calculations employ this method.

D. Comparison with Data

Spectroscopic amplitudes were calculated from the 12.5p + ^{17}O wave functions of Ref. 3 and from the DSD wave functions of Ref. 4. The numerical values for the various transitions analyzed are given in Table II. The DWBA calculations have been carried out with the optical parameter set combinations WSS-UPCR and GP-MS. For the spin-isospin exchange strength function[14] the values $|D(0,1)|^2 = 0.72$ and $|D(1,0)|^2 = 0.30$ were used. Values of $D_0^2 = 20 \times 10^4$ MeV^2 fm^3 and $D_0^2 = 34 \times 10^4$ MeV^2 fm^3 were assumed for the calculations with the two optical parameter set cominations WSS-UPCR and GP-MS, respectively. The angular distributions calculated with these numbers were individually normalized to the experimental differential cross sections for the presumed corresponding transitions (see Fig. 8). The quantity ε thus extracted are presented in Table III. As mentioned earlier, the DWBA calculations with both the WSS-UPCR and the GP-MS optical parameter set combinations give nearly identical angular distributions for all the transitions analyzed. Therefore in Figs. 6 and 7 only the results from the WSS-UPCR optical parameter set combination are presented. The DWBA curves shown in Fig. 6 are computed with the spectroscopic amplitudes from the 12.5 p + ^{17}O wave functions[3], whereas those shown in Fig. 7 result from calculations based on the DSD wave functions[4]. For the (p,^{3}He) reaction, the contributions to the complete calculated differential cross section (solid curves) from S=0, T=1 transfer (dotted curves) and S=1, T=0 transfer (dashed-dotted curves) are added incoherently.

IV. Discussion of the Individual Transitions

Figure 8 shows the experimental level scheme for the even parity states of the mirror ^{37}K-^{37}Ar pair up to an excitation energy of 5.5 MeV and for comparison the results of the two shell-model calculations mentioned earlier. The calculated levels have been identified with the experimental ones as indicated by the dashed lines.

1. Ground States (^{37}K and ^{37}Ar), $J^\pi = 3/2^+$

The experimental angular distributions exhibit characteristic L=0 patterns. Their shapes are well reproduced by the calculations, whereas the (p,t) strength is not accounted for. Recently[2] it was found that the ground state transitions of the (p,t) and (p,^{3}He) reactions on all $T_z = 1/2$ nuclei in the sd shell are systematically anomalous in the sense that for the (p,^{3}He) reaction the S=0, T=1 component of the predicted transfer strength, normalized to the mirror (p,t) cross section magnitude accounts for all of the strength observed. Therefore we believe that the values of ε (see Table III) for the (p,^{3}He) experimental to theoretical cross section ratio are accidentally close to unity. On the other hand, the (p,t) strength, which is less complex than the (p,^{3}He) strength, is underestimated by both sets of wave functions. However, the inclusion of about 10% $(f_{7/2})^2_{J=0,T=1}$ pick-up adding constructively to the sd-shell spectroscopic amplitudes can easily make up for this underestimation. Evidence for this amount of $(f_{7/2})^2$ admixture in the ground state wave function emerges from the excitation of odd-parity states in the $^{39}K(p,d)^{38}K$ reaction[17].

2. E_x=1.37 (^{37}K) and 1.41 (^{37}Ar) MeV, $J^\pi=1/2^+$

Both the (p,t) and (p,^{3}He) angular distributions exhibit L=2 patterns. Their shapes are well accounted for by the DWBA calculations based on both sets of shell-model wave functions. However, the T=1 transfer component is slightly underpredicted as can be seen from the (p,t) cross sections where ϵ is about 1.25. A slight increase of this T=1 transfer component gives a better agreement for the (p,t) cross section but has nearly no influence on the good agreement for the (p,^{3}He) cross section which is predominantly determined by the T=0 transfer component.

3. E_x=2.28 (^{37}K) and 2.22 (^{37}Ar) MeV, $J^\pi=7/2^+$

The selection rules allow for both the (p,t) and (p,^{3}He) reactions a mixture of L=2 and L=4. The experimental data exhibit a pure L=2 angular distribution for the (p,t) reaction and a mixed L=2 plus L=4 angular distribution for the (p,^{3}He) reaction. The (p,t) shapes are well accounted for by both sets of shell-model wave functions. However, the DSD wave functions underpredict the (p,t) strength by a factor of 2. On the other hand they predict the (p,^{3}He) differential cross section quite well with respect to both the shape and the magnitude. The 12.5p + ^{17}O wave functions overestimate slightly the (p,t) strength. For the (p,^{3}He) differential cross section they predict a too large L=2 transfer component which results in a somewhat poor fit to the experimental data. In addition the magnitude of the cross section is overpredicted. An inspection of the spectroscopic amplitudes in Table II shows that the discrepancy between the predictions of the two sets of wave functions results mainly from the larger value of the $(d_{3/2})^2_{3,0}$ transfer component yielded by the DSD wave functions.

4. E_x=2.75 (^{37}K) and 2.80 (^{37}Ar) MeV, $J^\pi=5/2^+$

The (p,t) transition can proceed by a mixture of L=2 and L=4, whereas for the corresponding (p,^{3}He) transition L=0, L=2 and L=4 are allowed. The experimental (p,t) and (p,^{3}He) angular distributions exhibit predominant L=2 and L=0 patterns, respectively. The 12.5p + ^{17}O wave functions describe these experimental patterns in general quite well, although the strong rise at forward angles in the (p,^{3}He) angular distribution is not reproduced. The strength of both the (p,t) and (p,^{3}He) cross section is underestimated by about a factor of 2. The DSD wave functions predict a too large L=4 component for the (p,t) transition which is in disagreement with the experimental data. Beyond that, the magnitude of the cross section is underpredicted by a factor of 3. While the general feature of the (p,^{3}He) angular distribution is reproudced, the magnitude is underestimated by a factor of 2.

5. E_x=3.24 (^{37}K) and 3.17 (^{37}Ar) MeV, $J^\pi=5/2^+$

The experimental (p,t) and (p,^{3}He) angular distributions show a predominant L=2 pattern with some small L=4 admixture as can be deduced from the filled L=2 minimum around 30°. The DSD wave functions underestimate this L=4 admixture (see Fig. 6), whereas the 12.5p + ^{17}O wave functions predict a too large L=4 contribution (see Fig. 7). For the corresponding (p,^{3}He) transition both sets of wave functions yield mixed L=2 and L=4 angular distribution which are dominated by the T=0 transfer component. These predictions are in clear disagreement with the experimental data which show less L=4 admixtures. In addition, inspecting Table III, the magnitude of the (p,^{3}He) cross section is underestimated by the DSD wave functions by nearly a factor of 2.

6. E_x=3.62 (^{37}K) and 3.60 (^{37}Ar) MeV, $J^\pi=3/2^+$

Both the (p,t) and (p,^{3}He) transitions proceed by a mixture of L=0 and L=2 transfer. The DWBA calculations based on both sets of wave functions predict a predominant L=2 transfer for the (p,t) transition and thus do not reproduce the data. Here, the inclusion of about 10% $(f_{7/2})^2_{0,1}$ transfer, as suggested for the ground state transition to improve the agreement between experiment and theoretical predictions, yields in a negligible increase of the L=0 admixture. The main contribution of the predicted (p,^{3}He) cross section comes from the T=0 transfer, which is forbidden in the corresponding (p,t) transition. The general feature of the (p,^{3}He) angular distribution, a mixture of L=0 and L=2 transfer, is reproduced by both sets of wave functions. The magnitudes of both the (p,t) and (p,^{3}He) cross sections are reasonably well predicted, as can be seen from Table III, although the fit of the (p,t) angular distribution is poor.

7. E_x=4.72 (^{37}K) and 4.73 (^{37}Ar) MeV, $J^\pi=7/2^+$

The experimental data for the two mirror transitions exhibit "pure" L=2 angular distributions, although L=4 admixtures are allowed by the selection rules. Both the 12.5p + ^{17}O and the DSD wave functions give a good account of the observed shapes. However, they overpredict the magnitude of the (p,t) and the (p,^{3}He) differential cross section by about a factor of 2.

8. E_x=5.05 (^{37}K) and 4.99 (^{37}Ar) MeV, $J^\pi 3/2^+$, T=3/2

Both the (p,t) and (p,^{3}He) transitions can only proceed by T=1 transfer. The experimental angular distributions exhibit characteristic

L=0 patterns. Their shapes are well reproduced by the DWBA calculations, although the 12.5p + ^{17}O wave functions predict a larger L=2 transfer component than the DSD wave functions resulting in a slightly inferior fit to the data. The magnitudes of the differential cross sections, however, are underestimated by about a factor of 2. Independent of this factor, the relative (p,t) to (p,^{3}He) cross sections are predicted correctly within 10%. As in the ground state transition, the inclusion of about 10% $(f_{7/2})^2_{0,1}$ pick-up adding coherently to the sd shell spectroscopic amplitudes can account for this discrepancy of a factor of 2 between the experimental and predicted strength.

V. Conclusions

In this paper a comparative study of the (p,t) and (p,^{3}He) reactions on ^{39}K was made with the aim of testing current shell-model wave functions of the states involved. Concurrently, the effects of uncertainties in the DWBA calculations, such as optical model parameters or form factor descriptions on these wave function tests were investigated. The DWBA results for the (p,t) and (p,^{3}He) reactions are strongly effected by small changes in the proton optical parameters whereas they were quite insensitive to the mass-3 parameters. Two different optical model parameter set combinations were adopted from the literature which describe the shapes of the experimental (p,t) and (p,^{3}He) angular distributions satisfactorily. Both proton parameter sets did not quite conform to the condition of fitting the elastic scattering cross section well. However, this has little or no effect on the DWBA analysis as far as realtive cross sections are concerned. These results justify the somewhat

artificial procedure of adjusting the optical model parameters in order to obtain good fits to the transfer data, since little significance can presently be attached to the absolute values of the calculated two-nucleon transfer cross sections. The use of the different methods of Drisko and Rybicki[12] and of Bayman and Kallio[13] for calculating the form factor resulted in nearly identical angular distributions, because the two methods produced form factors which are nearly equal in the region of the nuclear surface where the transfer reaction takes place.

Both the (p,t) and (p,^{3}He) differential cross sections were reproduced reasonable well by both sets of shell-model wave functions. The agreements with the experimental data are comparible to each other and to the results of similar shell-model DWBA analyses of two-nucleon transfer results in the sd shell. Some of the discrepancies between the observed and predicted strengths apparently stem from the omission of the $1f_{7/2}$ orbit in the model space.

REFERENCES

1. H. Nann, W. Benenson, W. A. Lanford, and B. H. Wildenthal, Phys. Rev. C10, 1001 (1974).
2. H. Nann and B. H. Wildenthal, Phys. Rev. Lett. 37, 1129 (1976).
3. B. H. Wildenthal, E. C. Halbert, J. B. McGrory, and T.T.S. Kuo, Phys. Rev. C4, 1266 (1971).
4. W. Chung and B. H. Wildenthal, unpublished.
5. F. D. Becchetti and G. W. Greenlees, Phys. Rev. 182, 1190 (1969).
6. I. S. Towner and J. C. Hardy, Advan. Phys. 18, 401 (1069).
7. H. W. Baer et al., Ann. of Physics (London) 76, 437 (1973).
8. P. P. Urone, L. W. Put, H. H. Chang, and B. W. Ridley, Nucl. Phys. A163,225 (1971).
9. B. A. Watson, P. P. Singh, and R. E. Segel, Phys. Rev. 182,977 (1969).
10. G. W. Greenlees and G. J. Pyle, Phys. Rev. 149,836 (1966).
11. H. P. Morsch and R. Santo, Nucl. Phys. 179, 401 (1972).
12. R. M. Drisko and F. Rybicki, Phys. Rev. Lett. 10, 275 (1966).
13. B. F. Bayman and A. Kallio, Phys. Rev. 156, 1121 (1967).
14. J. C. Hardy and I. S. Towner, Phys. Lett. 25B, 98 (1967).
15. P. M. Endt and C. van der Leun, Nucl. Phys. A214, 1 (19743).
16. P. J. Nolan, J. Physics G(London) 1, 35 (1975).
17. B. H. Wildenthal, J. A. Rice and B. M. Preedom, Phys. Rev. C10, 2184 (1974).

Table I. Optical-model parameters used in the DWBA calculations

	V (MeV)	r_R, a_R (fm)	W_v (MeV)	W_s (MeV)	r_I, a_I (fm)	V_{so} (MeV)	r_{so}, a_{so} (fm)
proton parameters							
Becchetti and Greenlees (BG)[5]	48.7	1.12,0.78	6.1	2.1	1.32,0.53	6.2	0.98,0.75
Watson, Singh and Segel (WSS)[9]	49.4	1.125,0.57		8.1	1.125,0.50	5.5	1.125,0.57
adapted from Greenlees and Pyle (GP)[10]	47.5	1.20.0.70		13.0	1.25,0.70		
mass-3 parameters							
Urone, Put, Chang, and Ridley (UPCR)[8]	171.6	1.14,0.74	20.4		1.56,0.77		
Morsch and Santo[11] (MS)	173.9	1.15,0.72	20.6		1.50,0.82		
bound state parameters							
BG-UPCR and GP-MS		1.25,0.65				λ=25.0	
WSS-UPCR		1.26,0.60				λ=25.0	

Table II. Spectroscopic amplitudes for $^{39}K \rightarrow A=37$

J_B^π	T_B		E_x^{th} (MeV)	J	T	(D5,D5)	(S1,S1)	(D3,D3)	(D5,S1)	(D5,D3)	(S1,D3)
$3/2^+$	1/2	(a)	0.00	0	1	-0.3333	-0.1546	-0.9609			
				2	1	-0.1040		-0.4297	-0.1202	-0.2020	-0.1169
				1	0	-0.1222	-0.0486	+0.5765		+0.1767	-0.1248
				2	0				-0.0057	-0.0492	-0.0069
				3	0	-0.0297		+0.8807	-0.0175	-0.1890	
		(b)	0.00	0	1	+0.3460	+0.1853	+0.9680			
				2	1	+0.1036		+0.4329	+0.1047	+0.1272	+0.1062
				1	0	+0.1080	+0.0463	-0.5808		-0.1221	+0.1384
				2	0				-0.0140	-0.0571	-0.0279
				3	0	+0.0266		-0.8872	+0.0278	+0.1502	
$1/2^+$	1/2	(a)	1.43	2	1	-0.0977		-0.3059	-0.1962	-0.2473	-0.3439
				1	0	+0.0111	-0.0258	-0.3059		+0.1926	+0.4052
				2	0				-0.1510	-0.3470	-0.3780
		(b)	1.28	2	1	-0.0769		-0.2049	-0.2034	-0.1716	-0.3902
				1	0	+0.0028	-0.0320	-0.2049		+0.1416	+0.4593
				2	0				+0.1553	+0.2197	+0.4267
$7/2^+$	1/2	(a)	1.98	2	1	+0.1869		+1.5545	+0.2548	+0.1647	+0.4261
				4	1	+0.0811				+0.3911	
				2	0				-0.0888	-0.2854	-0.2460
				3	0	+0.0477		-1.5545	+0.0420	+0.1479	
				4	0					-0.0316	
				5	0	+0.0227					

Table II. Cont'd.

J_B^π	T_B		E_x^{th} (MeV)	J	T	(D5,D5)	(S1,S1)	(D3,D3)	(D5,S1)	(D5,D3)	(S1,D3)
		(b)	2.23	2	1	+0.1235		+1.6668	+0.2079	-0.0590	-0.0033
				4	1	+0.0656				+0.2280	
				2	0				+0.0318	+0.1652	-0.0018
				3	0	+0.0402		-1.6668	+0.0085	+0.2042	
				4	0					-0.0717	
				5	0	+0.0178					
$5/2^+$	1/2	(a)	2.03	2	1	+0.1072		+0.6759	+0.0915	+0.2784	+0.2917
				4	1	+0.1175				+0.6371	
				1	0	+0.2310	+0.2506	-0.4617		-0.7455	-0.2450
				2	0				+0.1330	+0.3339	+0.3621
				3	0	+0.0806		+0.4936	+0.1167	-0.2513	
				4	0					+0.6005	
		(b)	2.39	2	1	+0.0669		-0.1685	+0.0299	+0.1568	+0.4354
				4	1	+0.1097				+0.6538	
				1	0	+0.1734	+0.3777	+0.1151		-0.8194	-0.4367
				2	0				-0.1014	-0.3319	-0.3527
				3	0	+0.0539		-0.1231	+0.0723	-0.0356	
				4	0					-0.6380	
$5/2^+$	1/2	(a)	3.04	2	1	+0.0792		+1.2200	+0.0465	+0.2414	-0.2411
				4	1	-0.0935				-0.3997	
				1	0	-0.0450	-0.1810	-0.8335		+0.4773	+0.2401
				2	0				-0.0649	-0.1978	-0.2000
				3	0	-0.0058		+0.8910	-0.0304	-0.3206	
				4	0					-0.2417	

Table II. Cont'd.

J_B^π	T_B		E_x^{th} (MeV)	J	T	(D5,D5)	(S1,S1)	(D3,D3)	(D5,S1)	(D5,D3)	(S1,D3)
		(b)	2.93	2	1	-0.1094		-1.3347	-0.1310	-0.1987	+0.1584
				4	1	-0.0230				-0.1443	
				1	0	-0.1239	-0.0266	+0.9117		+0.0878	-0.2119
				2	0				+0.0581	+0.1797	+0.0120
				3	0	-0.0352		-0.9747	-0.0519	+0.3911	
				4	0					+0.1920	
$3/2^+$	1/2	(a)	4.63	0	1	-0.0008	+0.1559	-0.0496			
				2	1	+0.1107		-0.0222	+0.2073	-0.3181	+0.5527
				1	0	-0.0854	-0.1224	+0.0298		+0.5135	+0.8398
				2	0				+0.0204	-0.1543	+0.2487
				3	0	+0.0030		+0.0455	+0.0571	-0.1991	
		(b)	3.24	0	1	+0.0259	-0.0275	+0.0612			
				2	1	-0.0981		+0.0274	-0.1653	+0.3082	-0.5396
				1	0	+0.0759	+0.2494	-0.0367		-0.4553	-0.8872
				2	0				+0.0693	-0.1293	+0.3009
				3	0	-0.0175		-0.0561	-0.0386	+0.2007	
$7/2^+$	1/2	(a)	4.67	2	1	+0.1946		-0.6719	+0.3568	+0.3183	+1.2717
				4	1	+0.0904				+0.4268	
				2	0				-0.2406	-0.4975	-0.7342
				3	0	+0.0338		+0.6719	+0.1498	-0.0440	
				4	0					+0.0737	
				5	0	+0.0533					

Table II. Cont'd.

J_B^π	T_B		E_x^{th} (MeV)	J	T	(D5,D5)	(S1,S1)	(D3,D3)	(D5,S1)	(D5,D3)	(S1,D3)
		(b)	4.09	2	1	+0.2256		-0.1530	+0.4487	+0.1803	+1.4984
				4	1	+0.0880				+0.2677	
				2	0				+0.2247	+0.2925	+0.8651
				3	0	+0.0470		+0.1530	+0.1766	-0.0024	
				4	0					-0.0376	
				5	0	+0.0426					
$3/2^+$	3/2	(a)	4.83	0	1	-0.2634	-0.1094	-0.9597			
				2	1	+0.1212		+2.1460	+0.1473	+0.1136	+0.0827
		(b)	4.91	0	1	+0.2908	+0.1665	+0.9604			
				2	1	-0.1089		-2.1475	-0.1574	-0.0368	+0.0260

(a) 12.5p + ^{17}O wave functions (Ref. 3)

(b) DSD wave functions (Ref. 4)

Table III. Comparison of the experimental and theoretical cross sections to states in ^{37}K-^{37}Ar.

$E_x(^{37}K)$ (MeV)	$E_x(^{37}Ar)$ (MeV)	J^π,T	E_x^{th} (MeV)		$\varepsilon = \sigma_{exp}/\sigma_{th}$ WSS-UPCR D_o^2=20				GP-MS D_o^2=34			
			(a)	(b)	(a)	(p,t) (b)	(p,^{3}He) (a)	(b)	(a)	(p,t) (b)	(p,^{3}He) (a)	(b)
0.00	0.00	$3/2^+,1/2$	0.00	0.00	2.55	2.40	1.30	1.20	2.35	2.18	1.03	1.03
1.37	1.41	$1/2^+,1/2$	1.43	1.28	1.20	1.26	0.95	1.00	1.24	1.35	0.91	1.00
2.28	2.22	$7/2^+,1/2$	1.98	2.32	0.83	2.15	0.60	0.83	0.82	1.99	0.59	0.82
2.75	2.80	$5/2^+,1/2$	2.03	2.39	1.65	3.00	2.40	2.06	1.65	3.34	2.35	1.96
3.24	3.17	$5/2^+,1/2$	3.04	2.93	1.20	0.70	0.95	1.70	1.17	0.74	1.02	1.70
3.62	3.61	$3/2^+,1/2$	4.63	3.24	0.60	0.85	1.30	1.15	0.68	0.91	1.29	1.06
4.72	4.73	$7/2^+,1/2$	4.67	4.09	0.70	0.43	0.48	0.40	0.73	0.46	0.47	0.39
5.05	4.99	$3/2^+,3/2$	4.83	4.91	2.20	1.70	2.10	1.80	2.00	1.76	1.91	1.69

(a) 12.5p + ^{17}O wave functions (Ref. 3)

(b) DSD wave functions (Ref. 4)

Figure Captions

Fig. 1 Spectra for the $^{39}K(p,t)^{37}K$ and $^{39}K(p,^{3}He)^{37}Ar$ reactions. Contaminant peaks are hatched.

Fig. 2 Angular distribution of elastically scattered protons on K. The curves are optical model results from various parameter sets discussed in the text.

Fig. 3 Angular distributions of the ground and first excited states transitions for the $^{39}K(p,t)$ and $^{39}K(p,^{3}He)$ reaction. The curves are DWBA results using different proton and mass-3 parameter set combinations. For further details see text.

Fig. 4 Reflection coefficients for the $^{39}K(p,t)^{37}K$ ground state transitions using various optical parameter sets.

Fig. 5 Angular momentum localization for the L=0 part in the $^{39}K(p,t)^{37}K$ ground state transition.

Fig. 6 Angular distributions for transitions to mirror final states in ^{37}K and ^{37}Ar populated in the $^{39}K(p,t)$ (upper half) and $^{39}K(p,^{3}He)$ lower half) reactions, respectively. The curves are DWBA calculations based on the DSD wave functions of Ref. 4.

Fig. 7 Angular distributions for $^{39}K(p,t)$ and $^{39}K(p,^{3}He)$ transitions to mirror final states. The curves represent DWBA calculations based on the 12.5p + ^{17}O wave functions of Ref. 3.

Fig. 8 Experimental and calculated energy-level schemes for ^{37}K-^{37}Ar. The experimental levels are mainly from Ref. 15. The spins are taken from Refs. 15 and 16.

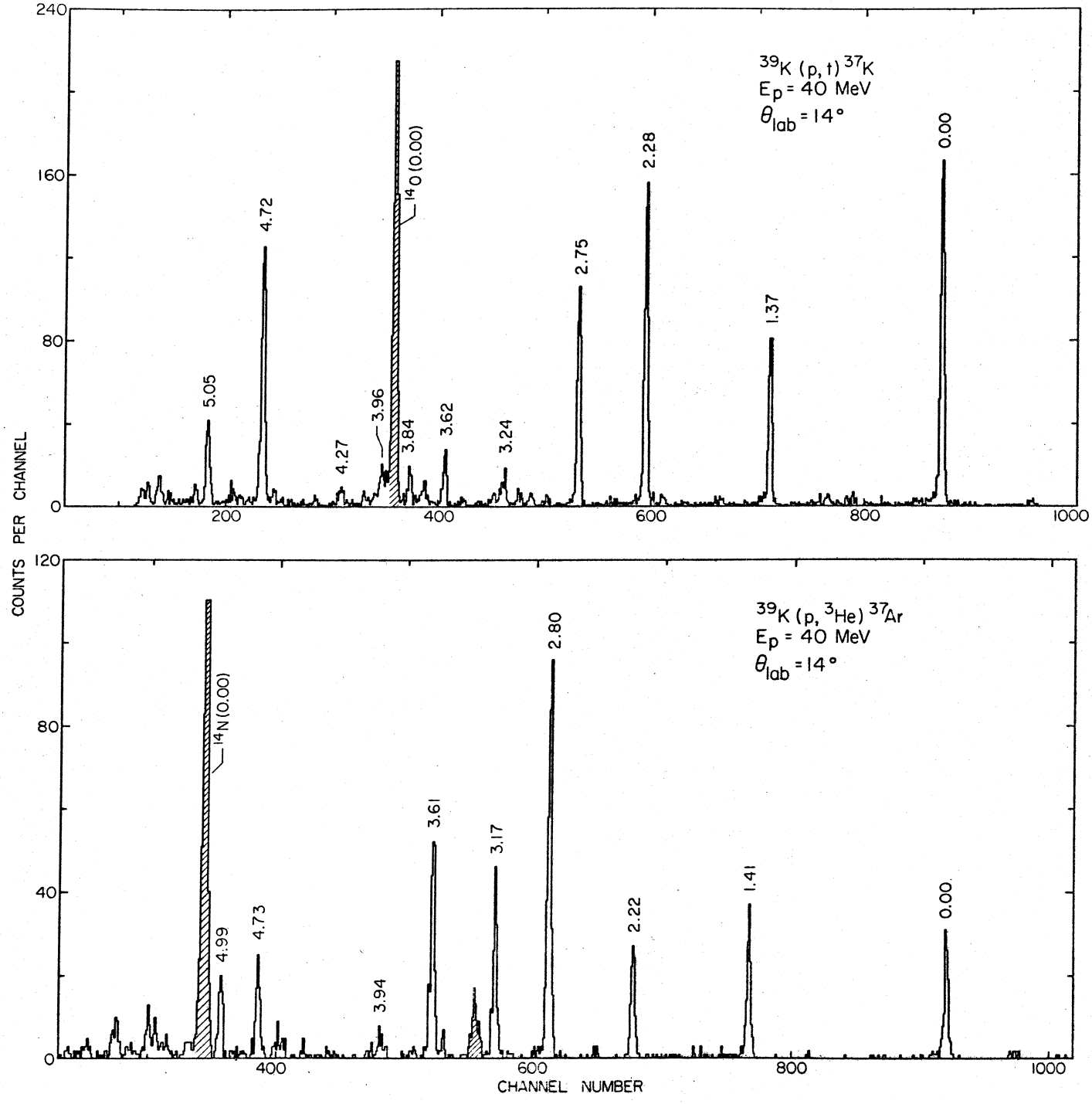
^{39}K (p, t) ^{37}K
E_p = 40 MeV
θ_{lab} = 14°
0.00
2.28
2.75
1.37
^{14}O (0.00)
4.72
5.05
4.27
3.96
3.84
3.62
3.24
^{39}K (p, ^{3}He) ^{37}Ar
E_p = 40 MeV
θ_{lab} = 14°
2.80
^{14}N (0.00)
3.61
3.17
4.99
4.73
3.94
2.22
1.41
0.00
COUNTS PER CHANNEL
CHANNEL NUMBER

Fig. 1

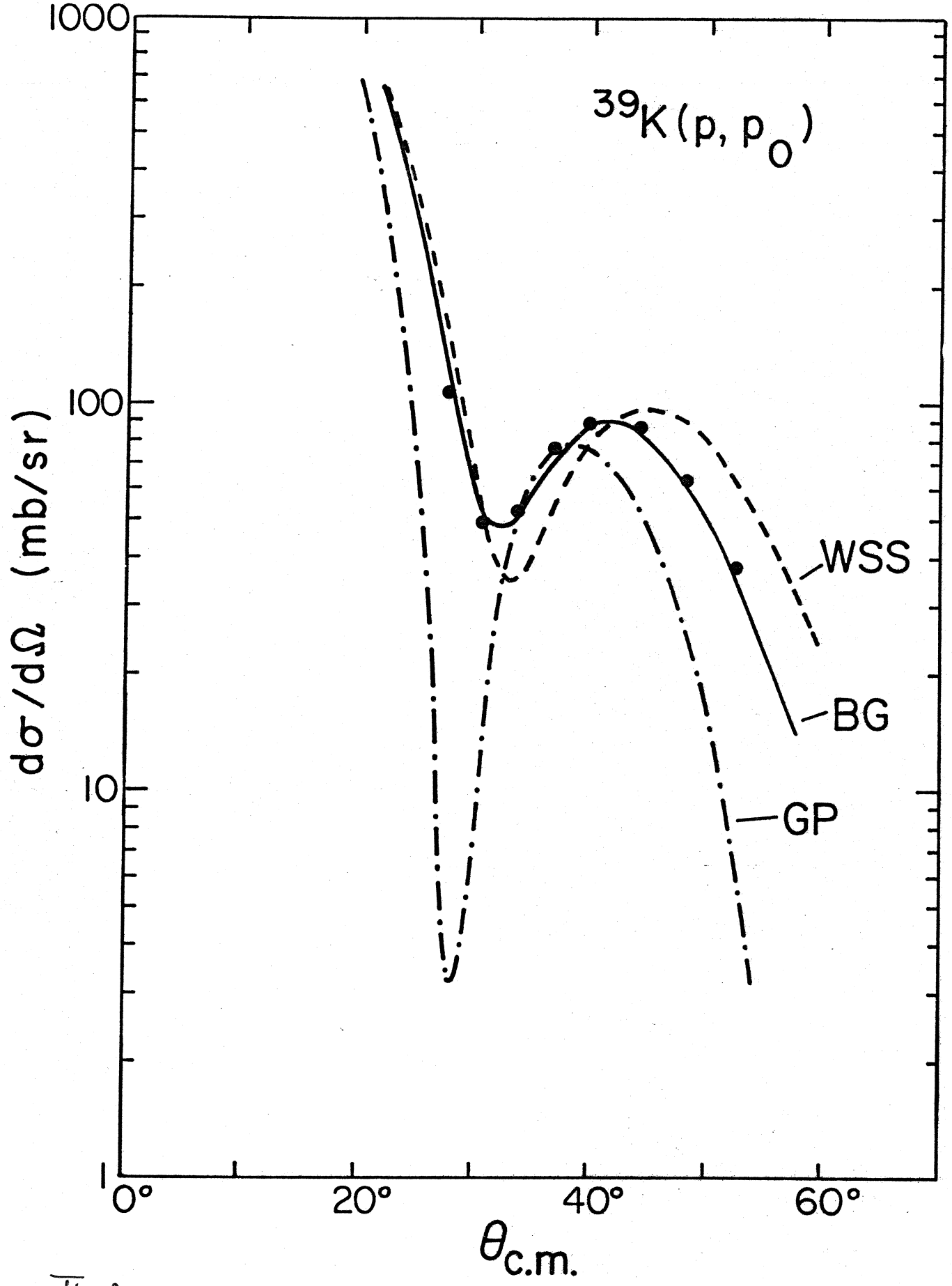
1000
100
10
1
$^{39}K(p, p_0)$
WSS
BG
GP
$d\sigma/d\Omega$ (mb/sr)
0°
20°
40°
60°
$\theta_{c.m.}$

Fig. 2

Fig. 3

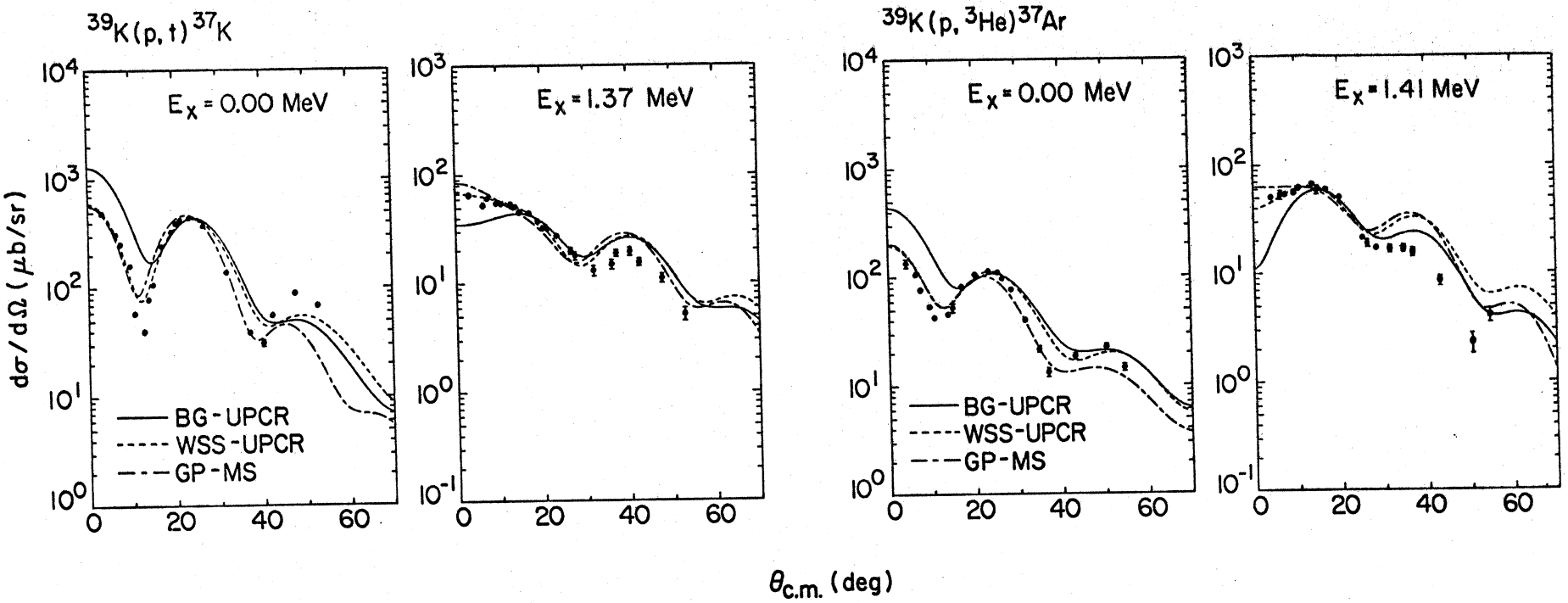
$^{39}K(p,t)^{37}K$
E_x = 0.00 MeV
E_x = 1.37 MeV
$^{39}K(p,{}^3He)^{37}Ar$
E_x = 0.00 MeV
E_x = 1.41 MeV
BG-UPCR
WSS-UPCR
GP-MS
$d\sigma/d\Omega$ (μb/sr)
$\theta_{c.m.}$ (deg)

Fig. 4

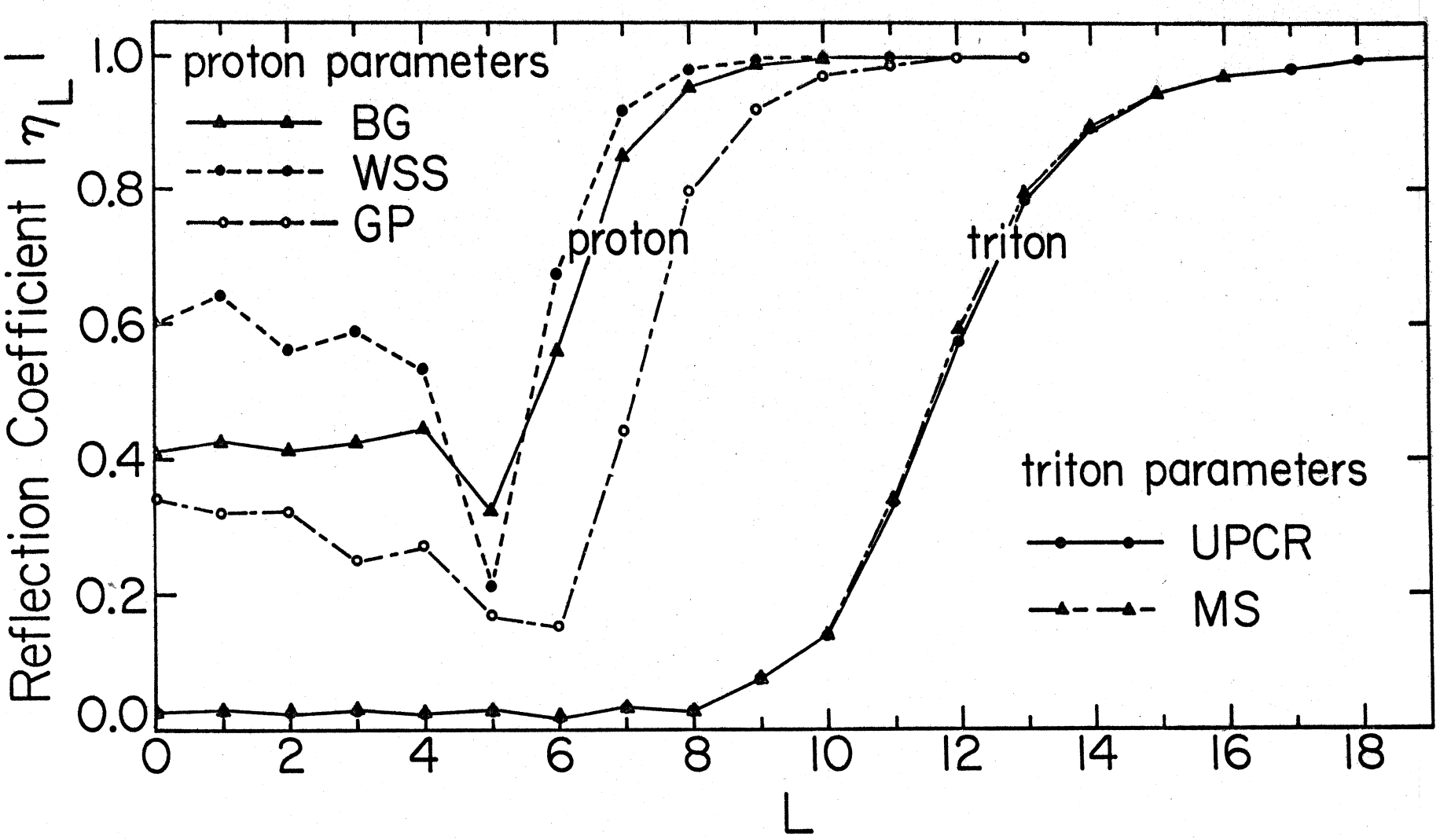
proton parameters
BG
WSS
GP
proton
triton
triton parameters
UPCR
MS
Reflection Coefficient $|\eta_L|$
L
1.0
0.8
0.6
0.4
0.2
0.0
0
2
4
6
8
10
12
14
16
18

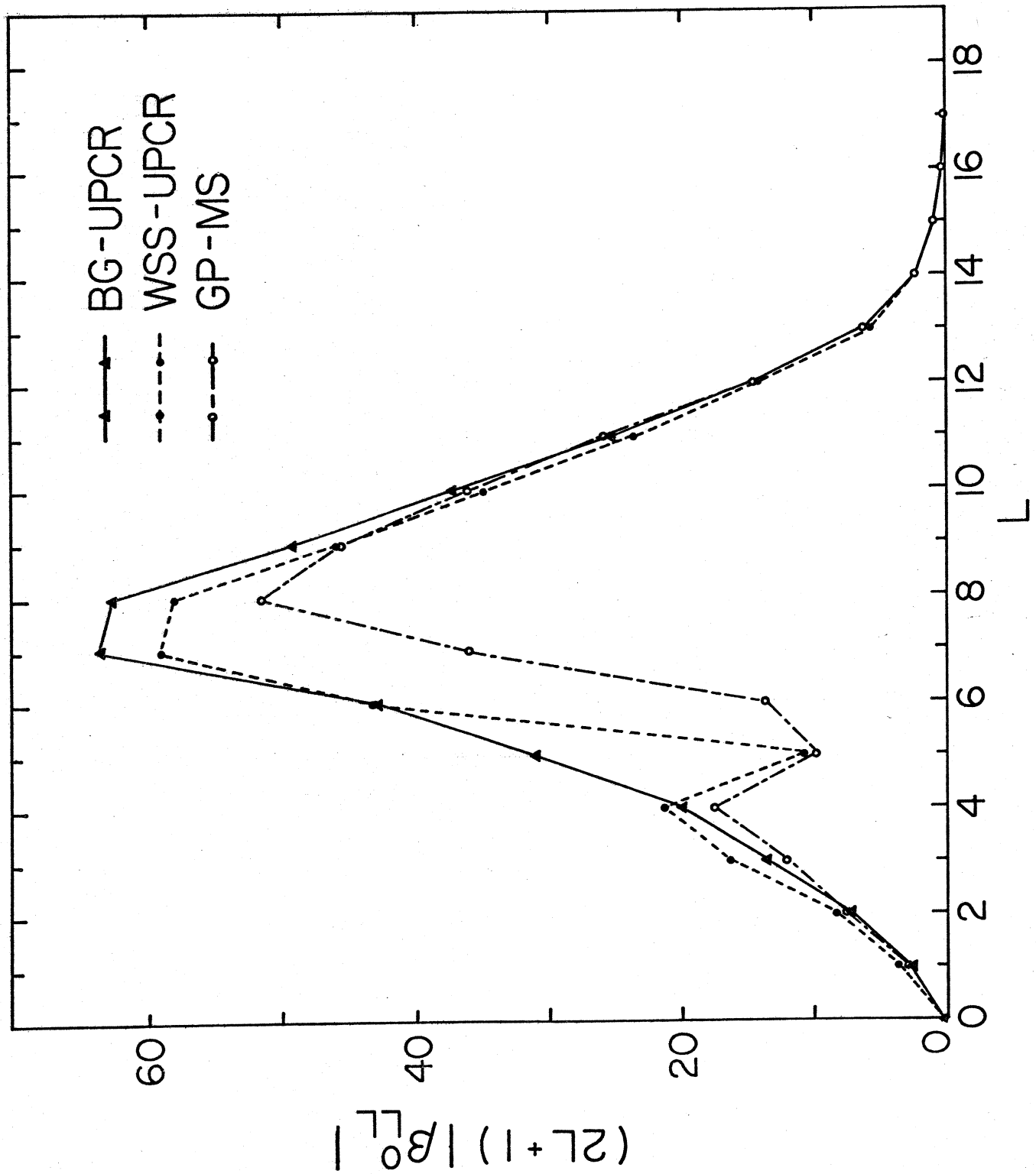

Fig. 5

Fig. 6

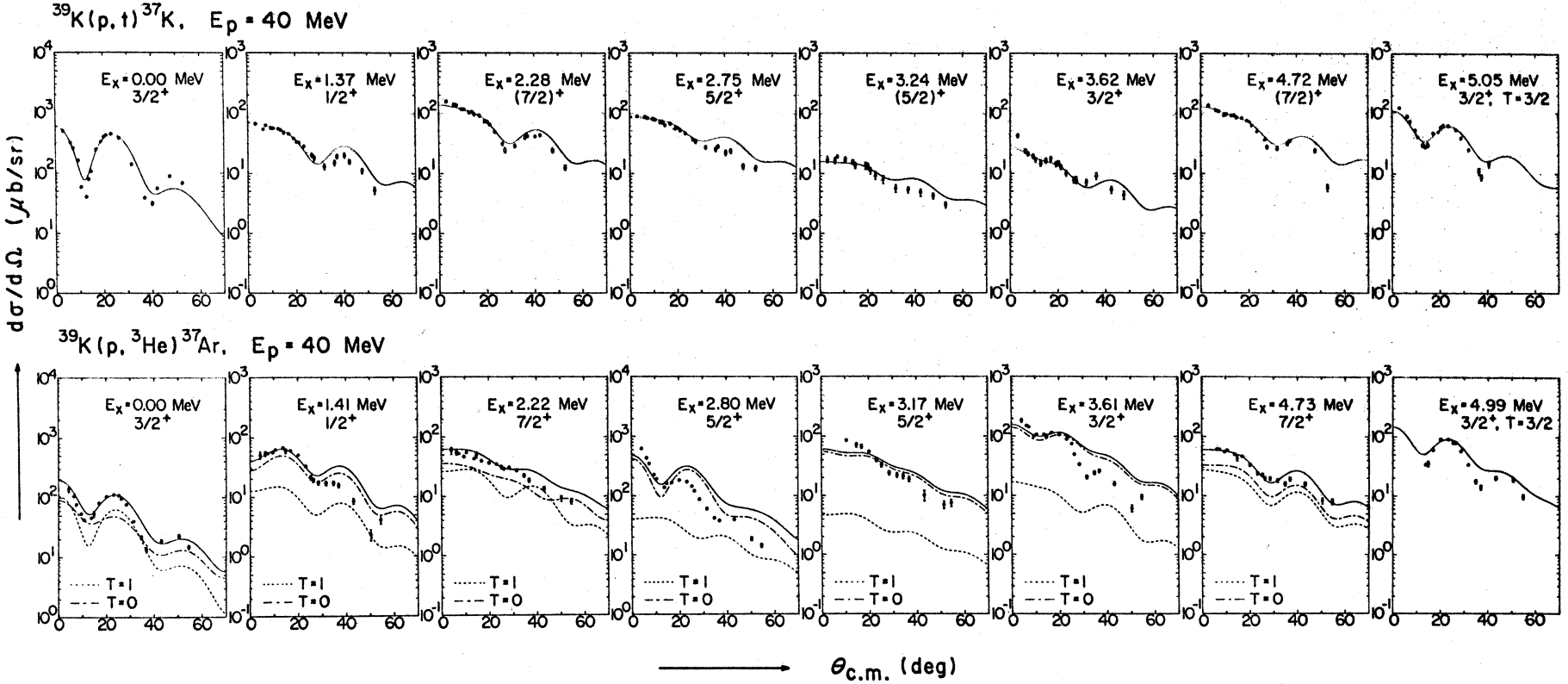
^{39}K(p,t)^{37}K, E_p = 40 MeV
E_x = 0.00 MeV 3/2$^+$
E_x = 1.37 MeV 1/2$^+$
E_x = 2.28 MeV (7/2)$^+$
E_x = 2.75 MeV 5/2$^+$
E_x = 3.24 MeV (5/2)$^+$
E_x = 3.62 MeV 3/2$^+$
E_x = 4.72 MeV (7/2)$^+$
E_x = 5.05 MeV 3/2$^+$, T = 3/2
^{39}K(p,^{3}He)^{37}Ar, E_p = 40 MeV
E_x = 0.00 MeV 3/2$^+$
E_x = 1.41 MeV 1/2$^+$
E_x = 2.22 MeV 7/2$^+$
E_x = 2.80 MeV 5/2$^+$
E_x = 3.17 MeV 5/2$^+$
E_x = 3.61 MeV 3/2$^+$
E_x = 4.73 MeV 7/2$^+$
E_x = 4.99 MeV 3/2$^+$, T = 3/2
T = 1
T = 0
dσ/dΩ (μb/sr)
$\theta_{c.m.}$ (deg)

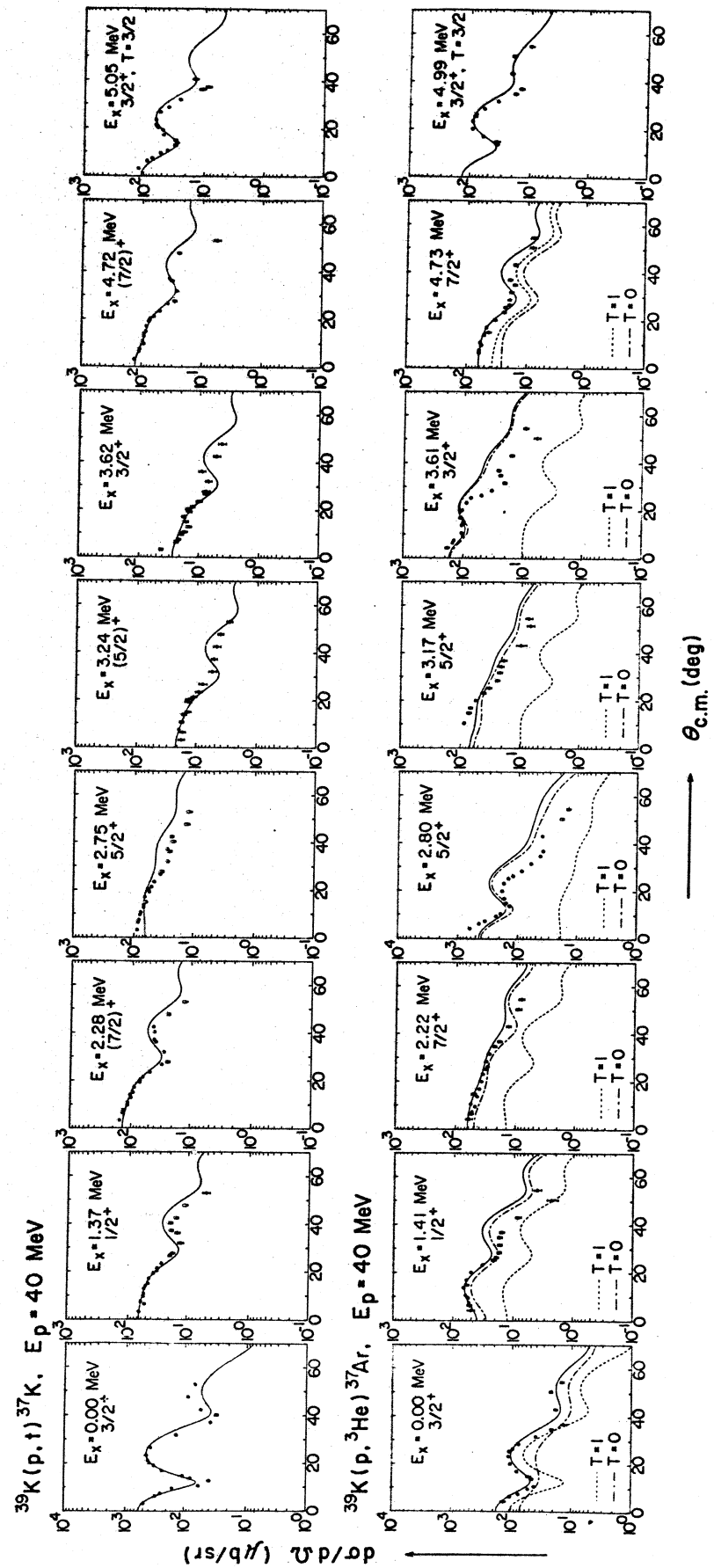
^{39}K(p,t)^{37}K, E_p = 40 MeV
^{39}K(p,^{3}He)^{37}Ar, E_p = 40 MeV
E_x = 0.00 MeV 3/2+
E_x = 1.37 MeV 1/2+
E_x = 2.28 MeV (7/2)+
E_x = 2.75 MeV 5/2+
E_x = 3.24 MeV (5/2)+
E_x = 3.62 MeV 3/2+
E_x = 4.72 MeV (7/2)+
E_x = 5.05 MeV 3/2+, T=3/2
E_x = 1.41 MeV 1/2+
E_x = 2.22 MeV 7/2+
E_x = 2.80 MeV 5/2+
E_x = 3.17 MeV 5/2+
E_x = 3.61 MeV 3/2+
E_x = 4.73 MeV 7/2+
E_x = 4.99 MeV 3/2+, T=3/2
T=1
T=0
dσ/dΩ (μb/sr)
θc.m. (deg)

Fig. 7

Fig. 8

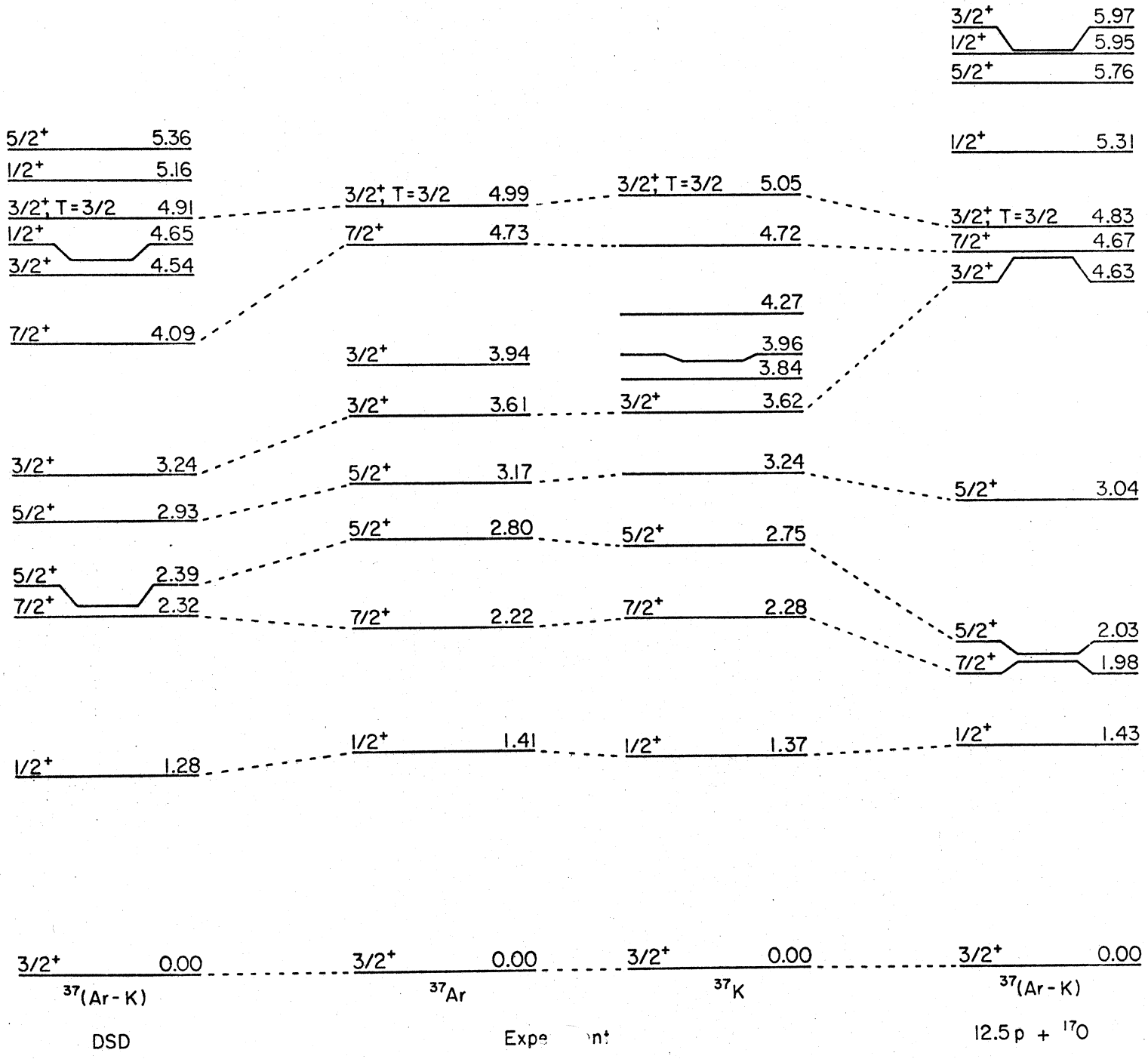
3/2+ 5.97
1/2+ 5.95
5/2+ 5.76
5/2+ 5.36
1/2+ 5.16
3/2+; T=3/2 4.91
1/2+ 4.65
3/2+ 4.54
7/2+ 4.09
3/2+ 3.24
5/2+ 2.93
5/2+ 2.39
7/2+ 2.32
1/2+ 1.28
3/2+; T=3/2 4.99
7/2+ 4.73
3/2+ 3.94
3/2+ 3.61
5/2+ 3.17
5/2+ 2.80
7/2+ 2.22
1/2+ 1.41
3/2+ 0.00
3/2+; T=3/2 5.05
4.72
4.27
3.96
3.84
3/2+ 3.62
3.24
5/2+ 2.75
7/2+ 2.28
1/2+ 1.37
3/2+ 0.00
1/2+ 5.31
3/2+; T=3/2 4.83
7/2+ 4.67
3/2+ 4.63
5/2+ 3.04
5/2+ 2.03
7/2+ 1.98
1/2+ 1.43
3/2+ 0.00
37(Ar-K)
37Ar
37K
37(Ar-K)
DSD
Expe nt
12.5p + 17O